Japanese Journal of Applied Physics

The Japan Society of Applied Physics

REGULAR PAPER

Impact of the effective refractive index in AlGaN-based mid-UV laser structures on waveguiding

Japanese Journal of Applied Physics **59**, 091001 (2020) **REGULAR PAPER**
https://doi.org/10.35848/1347-4065/abab44

Impact of the effective refractive index in AlGaN-based mid-UV laser structures on waveguiding

Qiang Guo[1*], Ronny Kirste[2], Pramod Reddy[2], Will Mecouch[2], Yan Guan[1], Seiji Mita[2], Shun Washiyama[1], James Tweedie[2], Zlatko Sitar[1,2], and Ramón Collazo[1]

[1]*Department of Materials Science and Engineering, North Carolina State University, Raleigh, North Carolina 27695, United States of America*
[2]*Adroit Materials, 2054 Kildaire Farm Rd, Suite 205, Cary, North Carolina 27518, United States of America*

[*]E-mail: qguo4@ncsu.edu

Received April 21, 2020; revised July 14, 2020; accepted July 31, 2020; published online August 13, 2020

The effective refractive index in optically-pumped 265 nm AlGaN-based lasers is assessed from the spacing of the longitudinal cavity modes in short laser cavities. It is found that the effective refractive index is significantly higher than the value estimated from the Sellmeier equation ($n = 2.5$) and reaches values of 2.9 and 3.2 for structures with 3 and 15 quantum wells, respectively. These results indicate that the Sellmeier equation underestimates the effective refractive index in AlGaN-based laser structures and that a different approach is needed for successful mid-UV laser modeling and design. © 2020 The Japan Society of Applied Physics

1. Introduction

Electrically-injected mid-ultraviolet (mid-UV) lasers are widely desired for applications in disinfection, non-line-of-sight communications, and biochemical sensing and defense.[1–5] Currently, the AlGaN material system in combination with native AlN substrates is the best candidate for electrically-injected mid-UV laser diodes.[6–8] While low-threshold optically-pumped lasing has been reported,[9] electrically-injected lasing below 300 nm has only recently been demonstrated.[10] For mid-UV laser diodes, AlGaN-based quantum structures, whose composition and design are chosen based on the wavelength of interest, form the active region (gain medium). Typically, the gain medium is sandwiched between a higher Al-composition waveguide and cladding layers. Unlike in the InGaN- or GaAs-based laser diodes, the waveguide and cladding layer design in the mid-UV AlGaN lasers is significantly limited by its electrical properties. While Si-doped Al-rich $Al_xGa_{1-x}N$ ($x \geqslant 0.85$) has a high donor activation energy and significant compensation, bringing about an upper limit for the cladding and waveguide Al composition,[11] *p*-AlGaN exhibits higher resistivity relative to *p*-GaN due to an increase in the activation energy of the Mg acceptor.[12,13] Thus, to obtain sufficient carrier injection into the active region of a ~265 nm laser, $Al_{0.65}Ga_{0.35}N$ is typically chosen as the waveguide and $Al_{0.75}Ga_{0.25}N$ as the cladding layer. Although it is optimal for carrier injection, this design decreases the refractive index contrast between the waveguide and the cladding layer, hence reducing the optical confinement, and increasing the mode leakage and laser threshold.[14]

In addition to the conventional *p*–*n* junction UV emitter design, and despite many added challenges, impracticality, and low efficiency limits, electron beam (e-beam) pumped AlGaN-based emitters have been considered as an alternative approach to mid-UV LDs.[15–19] The main allure of e-beam excitation is the avoidance of the hole injection challenges. Oto et al.[15] reported a high power efficiency of 40% for an AlGaN MQW (one should note that this is about twice the theoretical quantum limit of this concept, which does not even take into account additional cooling requirements) with emission wavelength around 240 nm. Hayashi et al.[17] first demonstrated an e-beam pumped UV laser at 353 nm. However, due to poor electron–hole pair generation by the e-beam, the threshold was four times higher than for optical pumping. To enhance carrier collection, a thick active region (~500 nm) was typically designed with the number of QWs ranging from 10 to 60,[13–17] making the total thickness of the MQW region comparable with or even larger than the thickness of the waveguide/cladding layers.

In order to address these mid-UV laser diode device challenges, simulations of the optical and electrical properties are widely performed and considered. Since the experimental data on refractive index dispersion of AlGaN is incomplete,[20,21] various simulation approaches employ extrapolated and approximated dispersion relations using the Cauchy and Sellmeier expressions.[22] However, the Cauchy expression assumes transparency, and the Sellmeier expression diverges at the resonance wavelength (i.e. the emission wavelength of the quantum structure). This was validated for select AlGaN compositions experimentally by spectroscopic ellipsometry, which confirmed a high refractive index at the proximity to the dielectric function critical points.[23,24] Hence, neither expression adequately describe the refractive index at wavelengths close to the bandgap, which is needed to simulate the mode confinement and overlap in laser structures. For example, AlN has a higher refractive index of 2.8 at 6 eV as derived from the dielectric function, as compared with the value of 2.5 derived from the Sellmeier equation.[25,26] This result indicates that the gain medium and potentially the waveguide have a much higher refractive index than the Sellmeier equation predicts. Therefore, knowing the effective refractive index and understanding the effects of the gain medium on the optical confinement and waveguiding is an important missing parameter in the design of AlGaN lasers.

In this work, we study the influence of the number of QWs (gain medium thickness) on the effective refractive index (n_{eff}) of the guided mode to obtain reliable refractive index dispersion data for the simulation of the optical mode overlap with gain medium and its confinement in the mid-UV laser structures that will enable tailored waveguide and gain medium designs. First, n_{eff} is estimated from the longitudinal mode spacing in short laser cavities. It is found that n_{eff} can reach values of ~3, which indicates that the Sellmeier equation greatly underestimates the refractive index of

AlGaN close to its dielectric function critical point. Next, we show that, with an increase in the number of quantum wells from 3 to 15, the laser light will be completely confined in the quantum well structure and n_{eff} is found to represent the refractive index of the gain medium ($n_{\mathrm{eff}} \sim 3.2$). Lastly, using this experimentally determined n_{eff}, the overlap integral between the gain medium and optical mode is calculated for both optically- and electrically-pumped laser structures. The results show that a higher refractive index in the gain medium contributes to additional optical confinement for mid-UV AlGaN lasers.

2. Experiments

AlGaN laser structures designed for optical pumping with varying number of QWs were grown via low-pressure metalorganic chemical vapor deposition (LP-MOCVD) on *c*-plane AlN single crystal substrates. The samples were grown following the same general structure: first, a 500 nm AlN homoepitaxial-layer was grown on bulk AlN, followed by a 150 nm or 500 nm thick $Al_{0.65}Ga_{0.35}N$ waveguide ($E_g = 5.1$ eV), $Al_{0.55}Ga_{0.45}N$/AlN (3 nm/4 nm) MQWs that were capped with 4 nm of AlN. The MQW structure was positioned close to the surface to enable optical pumping. The AlGaN composition, quantum well width, and barrier thickness were determined by high-resolution X-ray diffraction measurements and high resolution cross-section TEM imaging.[7] Details on the MOCVD growth process and AlN substrate preparation can be found elsewhere.[27–30]

Laser cavities were obtained by cleaving the AlN wafer along the *m*-plane. An ArF excimer laser ($\lambda = 193$ nm) was used to optically pump the laser cavities at room temperature. The laser output was recorded using a Princeton Instruments Acton SP2750 0.75 m monochromator in combination with a high resolution UV-grating (resolution 0.005 nm). Details of the optical pumping setup can be found elsewhere.[3,7,31]

3. Results and discussion

Figure 1 shows high-resolution lasing spectra for a 160 μm long laser cavity for different excitation power densities. The 10× MQW was grown on a 500 nm thick waveguide.

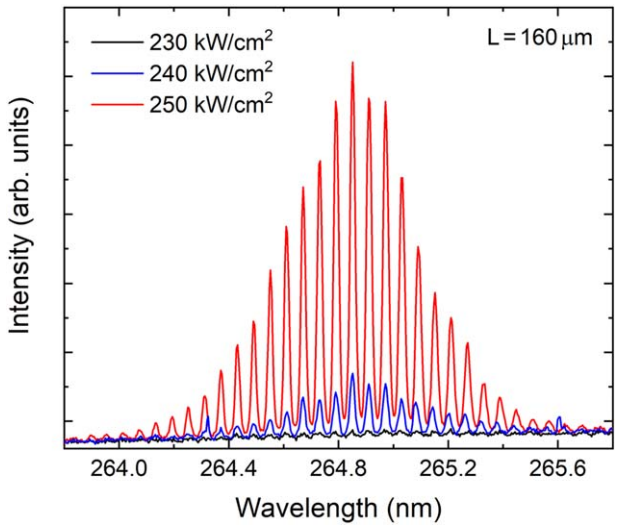

Fig. 1. (Color online) Power-dependent spectra of a 160 μm long laser cavity of an $Al_{0.55}Ga_{0.45}N$/AlN MQW structure (10 × MQW on 500 nm thick waveguide).

Well-resolved and equally-spaced longitudinal modes can be clearly observed at the emission wavelength centered at ~265 nm. The shape of the cavity mode profile follows the gain profile, indicating that only the amplified cavity modes will persist in the cavity. Furthermore, with an increase in the power density, the shape of the mode profile does not change significantly, while the light intensity shows a non-linear increase, indicative of lasing. It is worth noting that, under a high excitation power density (250 kW cm^{-2}), a high carrier density generated in the gain medium will cause a change in the absorption coefficient for the gain medium. Following the Kramers–Kronig relationship, the real part of the refractive index is connected to its imaginary part (extinction coefficient), and thus the absorption coefficient. Therefore, the refractive index will change with the excitation power density, however, carrier-induced refractive index change, even when accounting for heating, was found to be negligible, with the magnitude of $\Delta n \approx 10^{-4}$. This result is similar to that found in a previous study on InGaN lasers.[32]

The relative spacing, $\Delta\lambda/\lambda$, of the longitudinal cavity modes is given by the Fabry–Perot Eq. (1)[33]

$$\frac{\Delta\lambda}{\lambda} = \frac{\lambda}{2Ln_{\mathrm{eff}}}\left(1 - \frac{\lambda}{n_{\mathrm{eff}}}\frac{dn_{\mathrm{eff}}}{d\lambda}\right)^{-1}, \tag{1}$$

where λ is the emission wavelength, L is the cavity length, n_{eff} is the effective refractive index of the waveguide including the gain medium, and $\frac{dn_{\mathrm{eff}}}{d\lambda}$ is its dispersion. Although the dispersion term in Eq. (1) can be neglected in some material systems, AlGaN alloys exhibit a very strong dispersion, which causes a significant reduction in mode spacing. Thus, the dispersion of AlGaN needs to be taken into account in Eq. (1) when extracting n_{eff}.

Figure 2 shows the longitudinal mode spectral for the same structure but with cavity lengths of 120 and 290 μm.[34] As expected, for the longer cavity, the spacing between the two neighboring cavity modes becomes shorter and the peaks become narrower. The mode spacing, $\Delta\lambda$, and full-width-at-half-maximum, decrease from 0.07 to 0.032 nm and from 0.028 to 0.014 nm, respectively.

Figure 3 shows the relative mode spacing, $\Delta\lambda/\lambda$, as a function of the cavity length, L, for MQW structures with 3 and 15 quantum well pairs. In agreement with Eq. (1) the *x*-axis in Fig. 3 uses reciprocal units ($1/L$). The mode spacing, $\Delta\lambda$, is estimated from the average of five neighboring cavity modes near the center of the spectra. The cavity length was measured by using an optical microscope with accuracy better than ±10 μm. The effective refractive index, n_{eff}, was estimated from the slope of a linear fit to the relative mode spacing ($\Delta\lambda/\lambda$) as a function of $\lambda/2L$. Even though a large deviation between the Sellmeier equation and the real refractive index is expected at the bandgap energy, the Sellmeier equation still properly describes the wavelength-dependent refractive index behavior at longer wavelengths (i.e. $Al_{0.65}Ga_{0.35}N$ at a wavelength of 265 nm). Thus, the first-order derivative of the Sellmeier equation, $\frac{dn_{\mathrm{eff}}}{d\lambda} = -2.9\ \mu\mathrm{m}^{-1}$, was taken as the dispersion value for the $Al_{0.65}Ga_{0.35}N$ waveguide.[26]

The error for the effective refractive index comes from the variation of the cavity length ($-\frac{\lambda^2}{2L\Delta\lambda}\frac{\delta L}{L}$) as well as uncertainty in wavelength and fitting errors (negligible). The

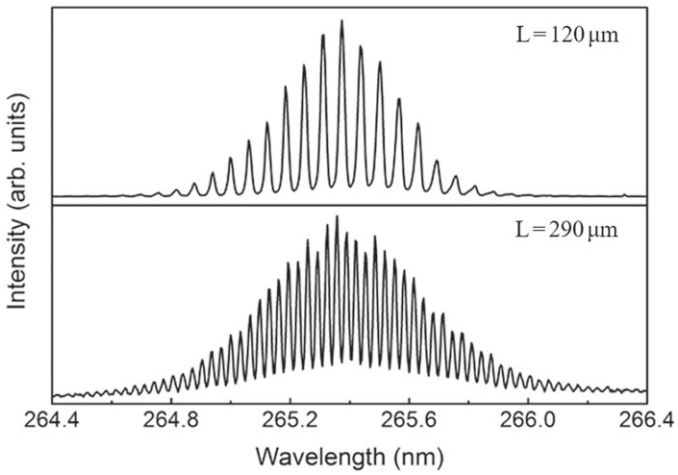

Fig. 2. High resolution spectra of 120 and 290 μm long laser cavities pumped above lasing threshold for an $Al_{0.55}Ga_{0.45}N$/AlN MQW structure.[34)]

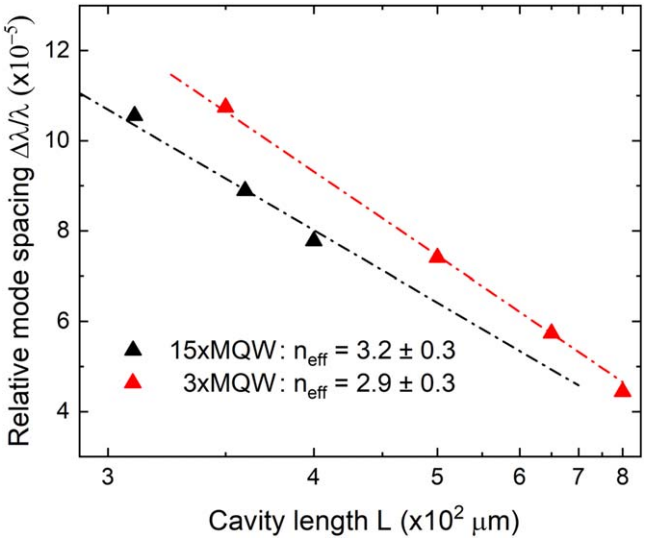

Fig. 3. (Color online) Relative mode spacing ($\Delta\lambda/\lambda$) as a function of the cavity length (L) for AlGaN/AlN MQW with 3 and 15 pairs, respectively. Dashed lines are best fit of Eq. (1) with indicated n_{eff}. Note that in agreement with Eq. (1) the x-axis is plotted in reciprocal scale, but that the actual length of the cavity was indicated.

wavelength variation can further be broken down into a longitudinal mode term ($\frac{\lambda^2}{L\Delta\lambda}\frac{\delta\lambda}{\lambda}$, term 1 $\frac{\lambda^2}{2L\Delta\lambda}$) and a dispersion term ($\lambda\delta\lambda\frac{d^2n_{\text{eff}}}{d\lambda^2}$, term 2 $\lambda\frac{dn_{\text{eff}}}{d\lambda}$). Then, the total error is the square root of summation of squares of error mentioned above. The error arising from the waveguide dispersion term to n_{eff} is given by $\lambda\delta\lambda\frac{d^2n_{\text{eff}}}{d\lambda^2}$, where λ is the emission wavelength of the laser and $\delta\lambda$ is the emission wavelength variation, which is estimated to be ±5 nm from the different cavities used for the experiments. In addition to the dispersion error, fitting errors, cavity length measurement error, and emission wavelength variation (±5 nm) from target wavelength 265 nm were also considered in the total error estimate. Using Fig. 3 and the described error estimation, we arrive at n_{eff} equal to 2.9 ± 0.3 and 3.2 ± 0.3 for quantum well structures with 3 and 15 pairs, respectively.

In the case of the quantum well structures with 3 pairs, light traveled in both the gain medium and waveguide and $n_{\text{eff}} = 2.9$ represents the effective refractive index for the whole laser structure. As the number of quantum wells increased while maintaining the waveguide thickness constant at 150 nm, the effective refractive index for the whole structure increased. For 15 quantum well pairs, the total gain medium thickness reached 105 nm, which corresponded to an optical thickness of ~300 nm for the 265 nm laser wavelength. In this case, the optical mode was mostly confined to the gain medium, making n_{eff} close to the average refractive index of the gain medium. This result is consistent with simulated light field distribution of an optically-pumped laser structure with 15 quantum well pairs.

To better understand the influence of refractive index of gain medium on the optical confinement factor, an overlap integral between the gain medium and the optical mode for the optically-pumped $Al_{0.55}Ga_{0.45}N$ QW structure with 3 quantum well pairs was calculated for both optically- and electrically-pumped lasers. Instead of using AlN barriers, $Al_{0.65}Ga_{0.35}N$ barriers were chosen in the simulation for both structures because AlGaN barrier enhances carrier injection for the electrically pumped structures. As shown in Fig. 4 (black curve), the overlap integral increased by a factor of five when the experimentally observed refractive index of 3.2 was used instead of 2.5 estimated from the Sellmeier

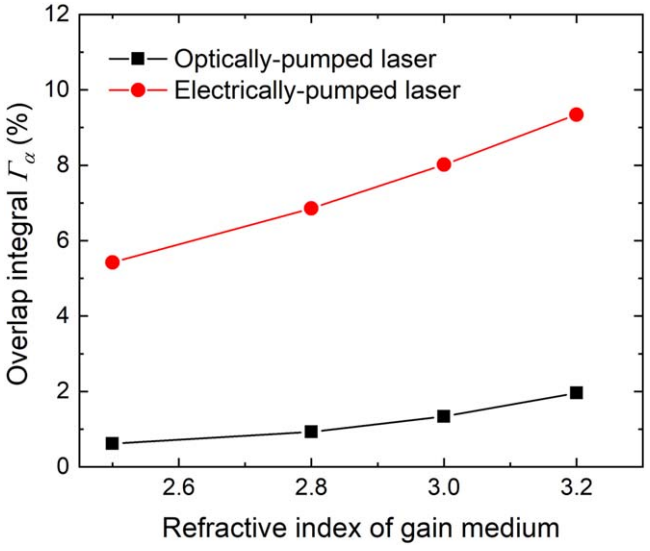

Fig. 4. (Color online) Gain medium-optical mode overlap integral, Γ_a, calculated for both optically and electrically pumped laser structures with 3 quantum wells as a function of the assumed effective refractive index.

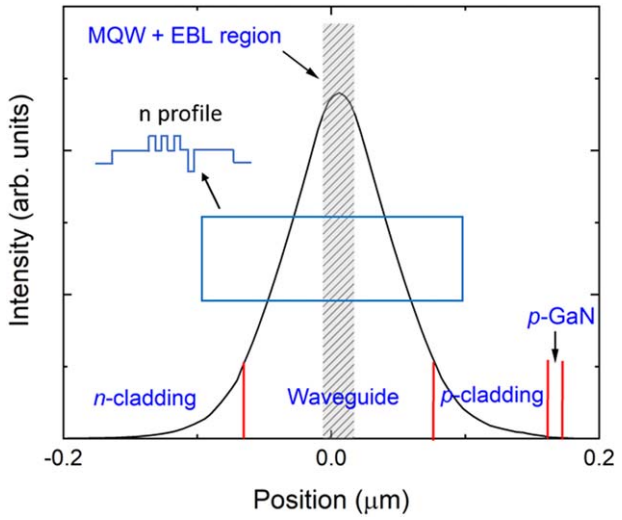

Fig. 5. (Color online) Light intensity distribution in the same electrically pumped UV laser structure shown in Fig. 4 as a function of position based on Silvaco simulation. The refractive index profile is indicated in the figure.

equation. Based on these data, an electrically-injected laser waveguide design that included an *n*-cladding layer ($Al_{0.75}Ga_{0.25}N$), *n*-waveguide ($Al_{0.65}Ga_{0.35}N$), 3 pairs $Al_{0.55}Ga_{0.45}N/Al_{0.65}Ga_{0.35}N$ MQW, electron blocking layer (EBL, $Al_{0.8}Ga_{0.2}N$), *p*-waveguide ($Al_{0.65}Ga_{0.35}N$), *p*-cladding ($Al_{0.75}Ga_{0.25}N$), and a thin *p*-GaN contact layer was simulated using Silvaco. Since the gain medium is now in the center of the waveguide, a much higher overlap of the optical mode with the gain medium is expected, as shown in Fig. 4 (red curve). One should note, that also in this case, the use of Sellmeier equation underestimates the overlap integral by a factor of 2.

Figure 5 shows the light distribution for a 265 nm AlGaN-based MQW laser structure based on Silvaco simulation. The shaded area indicates the overlap between the gain medium and the optical mode based on the refractive index profile indicated on the left. The maximum light intensity is achieved in the gain medium due to its highest refractive index, which is consistent with targeted design considerations. The overlap integral reaches about 10% for $n = 3.2$ derived from the optically pumped structures. These results indicate that although the $Al_{0.65}Ga_{0.35}N$ waveguide and $Al_{0.75}Ga_{0.25}N$ cladding layers exhibit a relatively low refractive index, the effective refractive index of the guided mode is significantly higher due to the contribution of the gain medium.

4. Summary

In summary, we estimated the effective refractive index from optically-pumped mid-UV AlGaN lasers. The method was based on measuring the spacing of the longitudinal laser modes in short cavities. Considering the emission wavelength and a dispersion $dn/d\lambda = -2.9\ \mu m^{-1}$ centered around 265 nm, the extracted effective refractive index reached values around 3. This is significantly larger than the value of $n = 2.5$ for $Al_{0.55}Ga_{0.55}N$ obtained from the Sellmeier equation. These results are crucial for proper AlGaN laser design as a higher effective refractive index in the gain medium will contribute additional optical confinement.

Acknowledgments

The authors acknowledge funding in part from NSF (ECCS-1508854, ECCS-1610992, ECCS-1653383, ECCS-1916800), ARO (W911NF-15-2-0068, W911NF-16-C-0101, W911NF-18-1-0415, W911NF-14-C-0008), AFOSR (FA9550-17-1-0225).

ORCID iDs

Qiang Guo https://orcid.org/0000-0002-3530-1888
Pramod Reddy https://orcid.org/0000-0002-8556-1178
Will Mecouch https://orcid.org/0000-0002-8317-5812
Shun Washiyama https://orcid.org/0000-0002-5095-6989
Zlatko Sitar https://orcid.org/0000-0002-7385-0837

1) T. Takano, Y. Narita, A. Horiuchi, and H. Kawanishi, Appl. Phys. Lett. **84**, 3567 (2004).
2) M. Martens et al., IEEE Photonics Technol. Lett. **26**, 342 (2014).
3) J. Xie et al., Appl. Phys. Lett. **102**, 171102 (2013).
4) R. Kirste, N. Rohrbaugh, I. Bryan, Z. Bryan, R. Collazo, and A. Ivanisevic, Annu. Rev. Anal. Chem. **8**, 149 (2015).
5) X.-H. Li et al., Appl. Phys. Lett. **106**, 41115 (2015).
6) Z. Bryan, I. Bryan, J. Xie, S. Mita, Z. Sitar, and R. Collazo, Appl. Phys. Lett. **106**, 142107 (2015).
7) R. Kirste, Q. Guo, J. H. Dycus, A. Franke, S. Mita, B. Sarkar, P. Reddy, J. M. LeBeau, R. Collazo, and Z. Sitar, Appl. Phys. Express **11**, 82101 (2018).
8) Q. Guo, R. Kirste, S. Mita, J. Tweedie, P. Reddy, S. Washiyama, M. H. Breckenridge, R. Collazo, and Z. Sitar, Jpn. J. Appl. Phys. **58**, SCCC10 (2019).
9) Q. Guo et al., "Design of AlGaN-based quantum structures for low threshold UVC lasers," J. Appl. Phys. **126**, 223101 (2019).
10) Z. Zhang, M. Kushimoto, T. Sakai, N. Sugiyama, L. J. Schowalter, C. Sasaoka, and H. Amano, Appl. Phys. Express **12**, 124003 (2019).
11) R. Collazo, S. Mita, J. Xie, A. Rice, J. Tweedie, R. Dalmau, and Z. Sitar, Phys. Status Solidi **8**, 2031 (2011).
12) M. L. Nakarmi, K. H. Kim, M. Khizar, Z. Y. Fan, J. Y. Lin, and H. X. Jiang, Appl. Phys. Lett. **86**, 92108 (2005).
13) M. Martens, C. Kuhn, T. Simoneit, S. Hagedorn, A. Knauer, T. Wernicke, M. Weyers, and M. Kneissl, Appl. Phys. Lett. **110**, 81103 (2017).
14) J. Piprek, *Nitride Semiconductor Devices Principle and Simulation* (Wiley, Berlin, 2007) Vol. 590.
15) T. Oto, R. G. Banal, K. Kataoka, M. Funato, and Y. Kawakami, Nat. Photonics **4**, 767 (2010).
16) D. Li, K. Jiang, X. Sun, and C. Guo, Adv. Opt. Photonics **10**, 43 (2018).
17) T. Hayashi, Y. Kawase, N. Nagata, T. Senga, S. Iwayama, M. Iwaya, T. Takeuchi, S. Kamiyama, I. Akasaki, and T. Matsumoto, Sci. Rep. **7**, 2944 (2017).
18) F. Fukuyo, S. Ochiai, H. Miyake, K. Hiramatsu, H. Yoshida, and Y. Kobayashi, Jpn. J. Appl. Phys. **52**, 01AF03 (2013).
19) S. V. Ivanov, V. N. Jmerik, D. V. Nechaev, V. I. Kozlovsky, and M. D. Tiberi, Phys. Status Solidi **212**, 1011 (2015).
20) M. Rigler, M. Zgonik, M. P. Hoffmann, R. Kirste, M. Bobea, R. Collazo, Z. Sitar, S. Mita, and M. Gerhold, Appl. Phys. Lett. **102**, 221106 (2013).
21) M. Rigler, J. Buh, M. P. Hoffmann, R. Kirste, M. Bobea, S. Mita, M. D. Gerhold, R. Collazo, Z. Sitar, and M. Zgonik, Appl. Phys. Express **8**, 42603 (2015).
22) J. W. Gooch, *Encyclopedic Dictionary of Polymers* (Springer, Berlin, 2010).
23) J. Wagner, H. Obloh, M. Kunzer, M. Maier, K. Köhler, and B. Johs, J. Appl. Phys. **89**, 2779 (2001).
24) C. Buchheim, R. Goldhahn, M. Rakel, C. Cobet, N. Esser, U. Rossow, D. Fuhrmann, and A. Hangleiter, Phys. Status Solidi **242**, 2610 (2005).
25) M. Röppischer, R. Goldhahn, G. Rossbach, P. Schley, C. Cobet, N. Esser, T. Schupp, K. Lischka, and D. J. As, J. Appl. Phys. **106**, 76104 (2009).
26) Ü. Özgür, G. Webb-Wood, H. O. Everitt, F. Yun, and H. Morkoç, Appl. Phys. Lett. **79**, 4103 (2001).
27) I. Bryan, A. Rice, L. Hussey, Z. Bryan, M. Bobea, S. Mita, J. Xie, R. Kirste, R. Collazo, and Z. Sitar, Appl. Phys. Lett. **102**, 61602 (2013).
28) I. Bryan, C. R. Akouala, J. Tweedie, Z. Bryan, A. Rice, R. Kirste, R. Collazo, and Z. Sitar, Phys. Status Solidi Curr. Top. Solid State Phys. **11**, 454 (2014).
29) R. Dalmau et al., J. Electrochem. Soc. **158**, H530 (2011).

30) J. Houston Dycus, S. Washiyama, T. B. Eldred, Y. Guan, R. Kirste, S. Mita, Z. Sitar, R. Collazo, and J. M. LeBeau, Appl. Phys. Lett. **114**, 31602 (2019).
31) W. Guo et al., J. Appl. Phys. **115**, 103108 (2014).
32) W. G. Scheibenzuber, U. T. Schwarz, T. Lermer, S. Lutgen, and U. Strauss, Appl. Phys. Lett. **97**, 21102 (2010).
33) U. T. Schwarz, E. Sturm, W. Wegscheider, V. Kümmler, A. Lell, and V. Härle, Phys. Status Solidi **200**, 143 (2003).
34) Z. A. Bryan, "Point defect identification and management for sub-300 nm light emitting diodes and laser diodes grown on bulk AlN substrates," PhD Thesis North Carolina State University (2015).